Scaling analysis, correlation length and compaction estimates of natural and simulated stylolites

D. Köehn, S. Köehler, Renaud Toussaint, I. Ghani, H. Stollhofen

Scaling analysis, correlation length and compaction estimates of natural and simulated stylolites

Koehn D. [1], Koehler S. [1], Toussaint R. [2,3], Ghani I. [4], Stollhofen H. [1]

[1] GeoZentrum Nordbayern, Friedrich-Alexander University (FAU) Erlangen-Nürnberg, Schlossgarten 5, 91054 Erlangen, Germany (daniel.koehn@fau.de)

[2] Université de Strasbourg, CNRS Institut Terre et Environnement de Strasbourg, UMR 7063, , 5 rue René Descartes, 67084 Strasbourg Cedex, France.

[3] SFF PoreLab, the Njord Centre, Department of Physics, University of Oslo, P.O. Box 1048 Blindern, NO-0316 Oslo, Norway

[4] Institute of Geology, University of the Punjab, Pakistan

Keywords:
stylolites, compaction, scaling, correlation length, roughness

Highlight:
- full scaling analysis of natural and numerical stylolites
- stylolites grow in 3 regimes with 3 characteristic length scales: grain-size, cross-over length and correlation length.

Abstract

Stylolites are rough dissolution surfaces that show three different scaling regimes in space and time. On the small scale surface energy dominates and stylolites roughen very slowly with a growth exponent of about 0.5 and a roughness exponent of about 1.0. On the intermediate scale elastic energy dominates and the surfaces roughening is happening faster with a growth exponent of about 0.8 and a roughness exponent of about 0.5. The transitional length between these two scaling regimes is determined by the stress during stylolite growth and is termed the cross-over length scale. On the

large scale another transition is reached beyond which the stylolite amplitude remains constant, this length scale is termed the correlation length. The correlation length is determined by time of growth or by the amount of compaction that happened at the interface as well as by the stylolite's system size. This length scale grows as a function of time and the dynamic exponent, which is about 2 in the surface energy dominated regime and 0.625 in the elastic energy dominated regime. We present examples of these scaling regimes for numerical as well as natural stylolites and show how the exponents can be used to determine the stylolite compaction through the different regimes. The numerical stylolites show an increase of correlation length as a function of system size in self-affine time series. Large samples of natural tectonic stylolites from the Franconian Alb (SE Germany) exhibit all three scaling regimes in a self-affine space series. The important length scales in the natural system are the grain size or noise at 30 μm, the cross-over length between the surface and elastic energy dominated regimes at 1.4 mm and the correlation length at 5.7 cm. The overall compaction on the tectonic stylolite is estimated to be in the range of 8 cm.

1. Introduction

Stylolites are rough dissolution surfaces that form by pressure solution. During their development, dissolution is localized at an interface when components (e.g. fossils, grains, clay drapes) of the rock dissolve slower than the rest and pin the interface (Stockdale, 1922; Park and Schot, 1968; Rispoli, 1981). The stylolite interface progressively roughens and grows in amplitude and wavelength and may collect material that dissolves slower. Stylolites have become the subject of quite a number of studies in the last 20 years (Toussaint et al., 2018) showing how they can be used as stress inversion tools (Schmittbuhl et al., 2004; Renard et al., 2004; Ebner et al., 2009a; 2010a, Rolland et al., 2012, 2014), to estimate paleo-burial depth (Ebner et al.,

2009a; Bertotti et al., 2017; Beaudoin et al., 2019; 2020a,b; Labeur et al., 2021), as indicators of tectonic regimes (Beaudoin et al., 2016), that they can be compared with calcite twin analysis (Beaudoin and Lacombe, 2018, Beaudoin et al., 2020c) and to estimate chemical compaction (Koehn et al., 2007, 2016; Laronne Ben-Itzhak, 2012). In addition, the properties of the stylolite interface in terms of anisotropic permeability and sealing or non-sealing capacities as well as their mechanical properties has been the matter of quite some debates (Koehn et al., 2016; Martin-Martin et al., 2018; Morad et al., 2018; Heap et al., 2018). In this contribution we are concerned with the roughening process itself as well as with compaction estimates using numerical simulations with the Elle-platform (Bons et al., 2008; Piazolo et al., 2019) as well as natural examples (Fig. 1). Our natural examples are tectonic stylolites from the Franconian Alb, in SE Germany north of the city of Kulmbach and close to the village of Kirchleus. The tectonic stylolites represent large rough surfaces that developed in Upper Jurassic (Malm) limestones (Fig. 1) in the vicinity of a seismic-scale fault (Kulmbach fault-zone). They are oriented perpendicular to bedding, forming vertical surfaces with a NNE-SSW orientation of teeth. The stylolites are associated with a Cretaceous compressional deformation that is thought to be lined with the Pyrenean fold and thrust belt (Kley and Voigt, 2008).

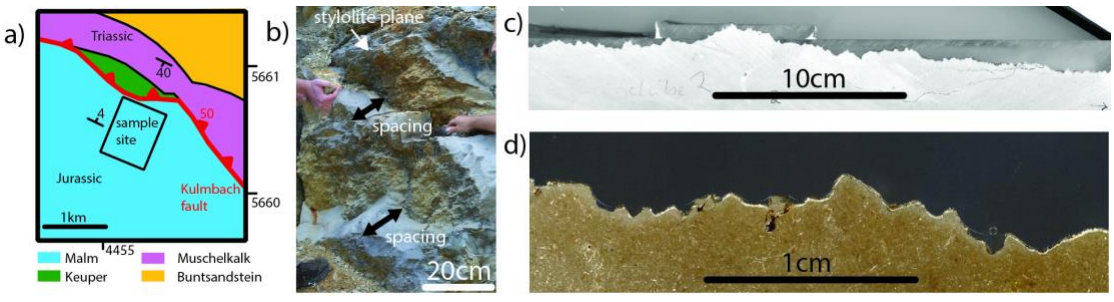

Fig. 1. a) Geological overview map of the sampling area with the Kulmbach reverse fault that displaces Triassic against Jurassic units. b) Sampling of tectonic stylolites in a Jurassic (Malm) limestone quarry in the Franconian Alb next to the Kulmbach fault near Kirchleus (50°10′ 49″ N, 11°22′ 11″ E) in SE Germany. c) 30 cm long slab that was used for the analysis. The sample is first prepared with epoxy and then cut to preserve the teeth. d) close up view of the stylolite surface under a digital microscope.

78

79 **1.1 Controls on stylolite roughness**

80 Roughening of surfaces falls into a range of dynamic scaling-functions of the so-
81 called Family-Vicsek scaling (Family and Vicsek, 1985) that is well known for a
82 range of processes including surface roughening, fluid infiltration in porous media,
83 development of flame fronts, fracture and fault surfaces, viscous fingering as well as
84 dynamics of bug colonies (Barabasi and Stanley, 1995; Laronne Ben-Itzhak, 2012;
85 Toussaint et al., 2018). All these processes develop structures that show a self-affine
86 scaling (they dynamic scaling) in space and time up to a correlation length after which
87 the roughness of the structure becomes constant. Self-similar and self-affine objects
88 are both termed fractal with the difference that a 2D self-similar object (the classical
89 fractal) scales the same on all scales in x and y, whereas a self-affine object scales
90 differently in x and y. For the specific case of rough surfaces like stylolites this means
91 that the width of the interface is a function of the length to an exponent *H*. If *H = 1.0*
92 the surface is self-similar, otherwise it is self-affine and changes as a function of the
93 scale. Typically, the interface is less rough on the larger scale (Fig. 1). The width or
94 amplitude of these interfaces (*w(l,t)*) as a function of length *(l)* and time *(t)* follows
95 the dynamic scaling law (Family and Vicsek, 1985; Laronne Ben-Itzhak, 2012)

96 $$w(l,t) \sim l^H f\left(\frac{l}{\chi}\right), \qquad \text{eq. 1}$$

97 where *l* is the sampling size or system size in simulations, χ the correlation length and
98 *H* the Hurst exponent of the self-affine scaling function. $f(u)$ with $u=l/\chi$ is a
99 universal scaling function with the following behaviour, if $u << 1$ then $f(u) =$
100 $const$, if $u >> 1$ then $f(u) = u^{-H}$. This means that if the sampling size *l* is smaller
101 than the correlation length χ the surface has the following behaviour (Laronne Ben-
102 Itzhak, 2012)

$$w(l,t) \sim l^H, \qquad \text{eq. 2}$$

where the roughness is a power law of the sampling size and independent of time. Within this scaling regime the roughness of a stylolite (it's width or amplitude) will become larger when a larger sample is taken. However, within this sample size the roughness has saturated, that means it will not change over time. The roughness can still evolve and flicker, but its width or amplitude will not change. On the other hand, if you take a large enough sample so that you are above the correlation length then the following applies (Laronne Ben-Itzhak, 2012)

$$w(l,t) \sim l^H \left(\frac{l}{\chi}\right)^{-H} = \chi^H = t^{\frac{H}{z}}, \qquad \text{eq. 3}$$

with *z* the dynamic exponent. At this length scale the roughness or width becomes constant. The correlation length will grow as a function of time until the system size is reached. For example, a very young stylolite has not developed a very rough surface and has a very small correlation length. With time the correlation length will grow and the stylolite will develop progressively larger wavelengths and amplitudes (Fig. 2). In simulations of stylolite roughening, where the system size is relatively small, the correlation length can reach the system size (Koehn et al., 2007). In these simulations, the roughening of the interface is induced by the dissolution of particles along an initial interface parallel to the x-dimension (Fig. 2). The system size is then represented by the number of elements (particles) along the x-dimension. Initially the correlation length will be the same as the model element size. Then both, correlation length and roughness start to increase. Eventually these length scales will reach the model system size if the stylolite grows long enough. At that point the roughness wavelength "sees" the boundaries of the system (left- and right-hand side of the simulation), it cannot produce larger wavelengths.

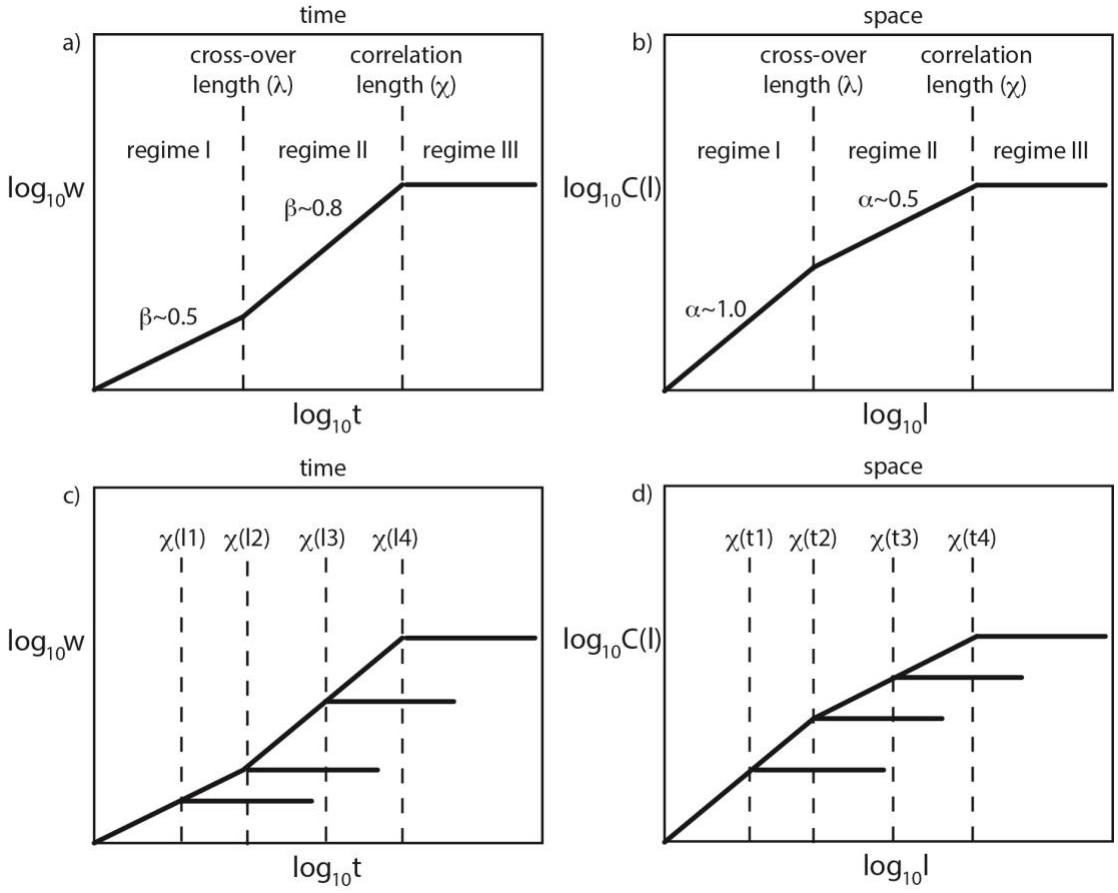

Fig. 2. Stylolite scaling in self-affine time and space series. a) time-series with three scaling regimes, two self-affine regimes with growth exponents β and a third regime where the stylolite width becomes constant. b) space-series with the same three scaling regimes where the two self-affine regimes are now characterized by the roughness exponent α. c) evolution of the correlation length χ as a function of system size l in the time-series. d) evolution of the correlation length χ as a function of time t in the space- series. Compilation of data and graphs from Barabasi and Stanley (1995), Koehn et al. (2007), Ebner et al. (2010b), Laronne Ben-Itzhak et al. (2012) and Toussaint et al. (2018).

Stylolites are relatively complicated interfaces that have an additional length scale separating two self-affine scaling regimes with different exponents (Fig. 2). These two regimes represent two energies in the system, both preferring a smooth interface and therefore, work against the roughening. On the small-scale surface energy is dominant, whereas on the large-scale elastic energy is dominating. The surface energy regime is also termed short-range interactions with the energy depending on the curvature of the interface whereas the elastic energy regime represents long-range interactions with the energy a function of the strain tensor of the deformed solid. Both of these energies scale differently, the elastic energy scales linearly with *l* whereas the

surface energy scales as *1/l*. The transition between these two energies is termed the cross-over length scale and can be used to determine the stress that was active while the stylolite roughened (Ebner et al., 2009a, 2010a). Stylolite roughening can be observed in self-affine time series in simulations and in self-affine space series in simulations and real samples. For the self-affine time series the average width is plotted in Fig. 2a in log-log against time (Koehn et al., 2007). This scaling exponent of width with time for a given length scale, $w(l,t) \sim t^{\beta}$ is called the growth exponent β. This scaling exponent has a value of about 0.5 in the surface energy dominated regime and 0.8 in the elastic energy dominated regime (Ebner et al., 2010b). This means that the stylolite grows very slowly in the surface energy dominated regime until the wavelengths are large enough to transition to the elastic energy dominated regime where growth is faster. For the self-affine space series the width is plotted in log-log against window size *l* (in Fig. 2b the width is represented by the correlation *C(l)*, Laronne Ben-Itzhak et al., 2012; Toussaint et al, 2018). The corresponding scaling exponent is termed the roughness exponent α, which is about 1.0 in the surface energy dominated regime and about 0.5 in the elastic energy dominated regime. In the surface energy dominated regime the surface is almost self-similar whereas in the elastic energy dominated regime the stylolite is rough on the small scale and flat on the larger scale (Fig. 1). This means that on the large outcrop-scale (1-50m) the stylolite surface is shown as a flat line, whereas it becomes very rough with a high amplitude to wavelength ratio from hand-specimen to thin-section scale (cm to mm). Once the interface reaches the cross-over length the scaling becomes self-similar with a roughness exponent of about 1.0, so that the amplitude to wavelength ratio does not change any more.

In this contribution we will present the full scaling analysis as time series on numerical stylolites where the system size changes from 50 to 100, 200 and 400 particles along the stylolite and as space series on a large natural stylolite sample that covers the full range of the three scaling regimes across five orders of magnitude.

2. Methods

2.1 Numerical Simulations

The numerical simulations were performed within the microstructural modelling environment "Elle" (Bons et al., 2008; Piazolo et al., 2019), where roughening of stylolite surfaces is modelled in 2D using a lattice-spring approach (Koehn et al. 2007, 2012, 2016; Ebner et al., 2009b). In this setup, a two-dimensional model box is filled with particles that are connected by linear elastic springs, where particles that are not connected by springs are still repulsive, so that they build up elastic stresses once they are pushed into each other. In the centre of the box one row of particles is removed and the boundary particles are defined as reactive meaning that they can dissolve. The model is stressed by a displacement-controlled movement of the upper and lower boundary of the box inwards so that particles meet at the reactive interface. Once particles touch, the elastic stress in the model is calculated using an over-relaxation algorithm where particles are moved until they are in an overall equilibrium position defined by a threshold (Allen, 1954). In the next step the dissolution rate D_i (m s^{-1}) of particle *i* at the interface is calculated according to Koehn et al. (2007)

$$D_i = k_i V_s \left(1 - exp \frac{-\Delta\sigma_n V_s - \Delta E_s - \Delta E_{el}}{RT}\right), \qquad \text{eq. 4}$$

with k_i (mol m^{-2} s^{-1}) as rate constant (that can vary per particle) and V_s (m^3 mol^{-1}) as the molecular volume, $\Delta\sigma_n$ (Pa) changes in normal stress at the interface relative to an average stress on the stylolite, ΔE_s (J m^{-3}) changes in surface energy at the interface,

194 ΔE_{el} (J m^{-3}) changes in elastic energy at the interface, R (J mol^{-1} ^{o}K^{-1}) is the universal
195 gas constant and T (^{o}K) is the absolute temperature. Changes in surface energy at the
196 interface are calculated as changes in surface energy per area unit on a single particle
197 at the interface where the surface energy is

198 $$E_s = \frac{\gamma}{\rho}, \qquad \text{eq. 5}$$

199 with γ the surface free energy (J m^{-2}) and ρ the local radius of curvature (m) with an
200 average across up to 40 neighbours along the interface (Koehn et al., 2007). The
201 elastic energy is calculated using the strain tensor (u_{ik}) from the lattice spring network
202 according to

203 $$E_{el} = \frac{1}{2}\lambda_1(\sum_i u_{ii})^2 + \lambda_2 \sum_{i,k}(u_{ik})^2, \qquad \text{eq. 6}$$

204 with λ_1 and λ_2 the Lamé constants (Pa).
205 Noise is inserted by a variation of k_i for single particles. In the model the dissolution
206 rate for all particles at the interface is calculated and the particle that dissolves fastest
207 is removed. The stress in the model is calculated again and the next particle is
208 removed until no more particle dissolves within a given time step. Then the boundary
209 condition of moving the upper and lower wall is applied again.
210 The model has several assumptions, such as 1) the dissolution starts at a flat interface,
211 2) the model only dissolves and assumes infinite matter transport and precipitation, 3)
212 the model does not really have an absolute time scale, 4) we are applying the
213 difference in normal stress at the interface and 5) the boundary conditions are
214 displacement controlled. 1) That dissolution starts at a flat interface is especially
215 reasonable for sedimentary stylolites that may start at bedding interfaces. Tectonic
216 stylolites may be more problematic because it is not clear how they are initiated.
217 However, they may start at existing joints or veins, which are probably flat interfaces
218 as well. 2) Fluid in the model is only indirectly treated, because we are only

concerned with the stylolite roughening. Therefore we assume that a fluid is present at all times and that transport of matter through diffusion in the fluid as well as precipitation are fast relative to dissolution and strain rate. The roughening process should be independent of the fluid as long as it is present, even though absolute timing may be affected if transport or precipitation become rate controlling. 3) The model only looks at dissolution and assumes infinite transport and precipitation, which limits the meaning of "time" in the model. However, for the scaling process the absolute time is not important but rather the dissolution at the interface. The dissolution and thus roughening is driven by the constant boundary condition in the model and thus the strain rate or displacement rate of the boundary. This relative time scale is used in the model with the absolute time not needed for the scaling analysis. On the contrary, the absolute time may even offset the scaling analysis in time, because the scaling analysis assumes a constant dissolution rate at the interface. 4) The application of the difference in normal stress at the interface assumes that the fluid is saturated with respect to the stress on the stylolite. With difference in normal stress we mean that we take an average of the normal stress along the whole stylolite and use the difference between the local stress on a particle relative to the mean normal stress as driving force. We assume at that point that transport by diffusion is slow relative to dissolution and thus relative to oversaturation of the fluid in the interface. We argue that this way of treating the dissolution is realistic because it produces that same scaling properties in simulations than those of natural stylolites. 5) Displacement controlled boundary conditions produce a constant driving force and can be used as equivalent time. A stress driven boundary condition may not produce a constant dissolution and is more complicated.

2.2 Natural Stylolites

As natural examples we use tectonic stylolites from a quarry in the Franconian Alb north of the village of Kirchleus (Fig. 1). These stylolites develop very well exposed large surfaces with a pronounced roughness so that large samples can be easily taken. In order to preserve the roughness of the interface, which is often destroyed during cutting and preparation of thin-sections, we preserved the whole surface with epoxy. Once the epoxy cover is finished the samples are cut preserving the original roughness down to the grain size (Fig. 1). We then scan the cut surfaces at high resolution with 30.000 pixels along 30cm of interface. In addition, we prepare 10 thin-sections along the interface (Fig. 1) to be able to resolve resolutions down to the grain size under a microscope.

2.3 Scaling

The scaling analysis of the numerical as well as the natural stylolites was undertaken using scripts in Matlab. For the numerical stylolites the interface per time step is converted to a line where every point in *x* has exactly one *z* (height) component. Then the mean width $w_{(l)}$ (m) of the interface is determined for each time step according to

$$w_{(l)} = \sqrt{\frac{1}{l}\sum_{i=1}^{l}\left[h_i - \bar{h}\right]^2}, \qquad \text{eq. 7}$$

with h_i (m) representing the height of point *i* on the interface and $\bar{h}$ (m) the average height of the interface. For the time-series the mean width is then plotted in log-log against time (model steps).

The natural stylolites were redrawn using the software GIMP, converted to grey-scale Jpg images and then converted to a line using Matlab scripts. For the space-series a height-height correlation function ($C(l)$) is used according to

$$C(l) \equiv \sqrt{\left[\left(h(x) - h(x')\right)^2\right]_l}, \qquad \text{eq. 8}$$

where h is the height of point x on the interface and l the distance between point x and x'. The function then gives an average height value across the interface for variable distances l and $C(l)$ is plotted in log-log against l.

3. Results

3.1 Numerical Simulations

We use the following parameters for the simulations: the average dissolution constant (D_i) for calcite is 10^{-4} mol/(m^2s), the molar volume for calcite (V_i) is 4 x 10^{-5} m^3/mol, the temperature (T) is 500 ºK, the surface free energy is 0.27 J/m^2, the Poisson ratio is 0.33, the Young's modulus is 40 GPa, the real physical width of the system is 10 mm, the universal gas constant is 8.3145 $Jmol^{-1}K^{-1}$ (Koehn et al., 2007; 2012). We use resolutions of 50, 100, 200 and 400 particles in the x-direction in about 50 runs and dissolve up to 2/3 of the model domain.

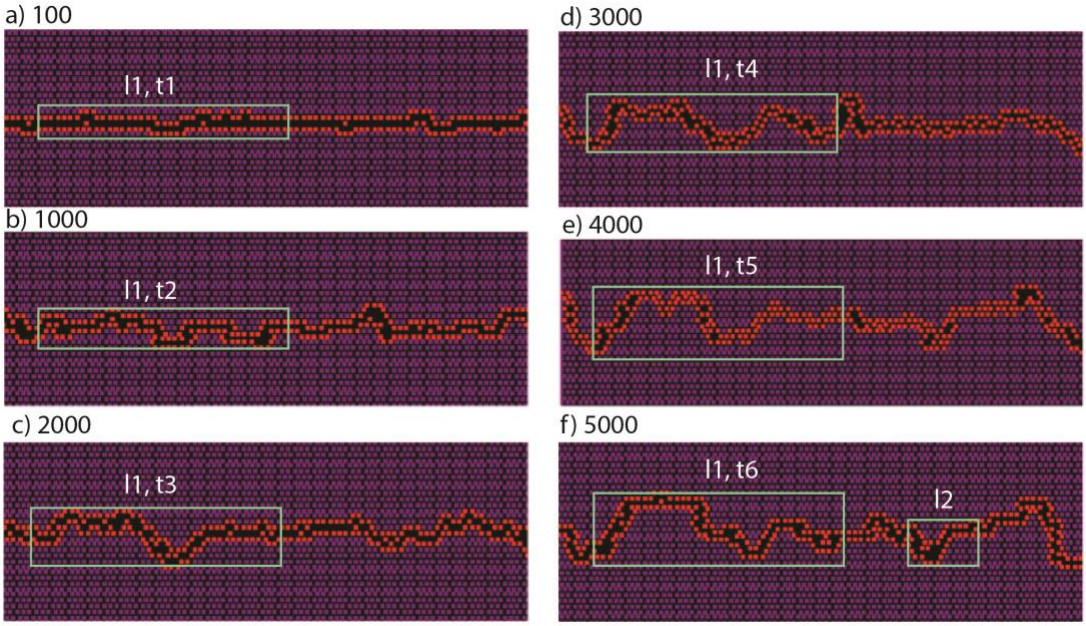

Fig. 3. Simulated stylolite with a resolution of 100 particles in x. The box is compacted vertically with a displacement controlled boundary. Particles can dissolve at an initially flat interface in the middle of the box as a function of local changes in elastic and surface energy as well as normal stress. Roughening develops during dissolution of particles as a function of a variation in dissolution constants. a) 100, b) 1000, c) 2000, d) 3000, e) 4000 and f) 5000 compaction steps. The large box shows the roughness evolution within the box as a function of time/compaction steps (t1-t6). The correlation length is reached at e) when the amplitude growth stops. In f) two boxes at length scale l1 and l2 are shown with the smaller box showing an earlier reached correlation length and thus a smaller amplitude within the box.

An example of a simulation with 100 particles in the x-direction is shown in figure 3 with the stylolite interface in red. The interface roughens progressively from stage 100 through stages 1000, 2000, 3000 and 4000. At this time the interface is still evolving but the amplitude growth has slowed down and there is no significant growth between stages 4000 and 5000. The scaling can also be illustrated by setting a rectangular window with a fixed width *(l_1)* on the stylolite so that the window covers the amplitude of the roughness. The height of the window increases progressively from model time steps 100 to 4000 *(t_1-t_5)* where the height remains constant. If we look at windows with different widths *(l_1, l_2)* at stage 5000 one can observe that the height of the window that covers the stylolite is smaller for smaller windows (Laronne Ben-Itzhak, 2012).

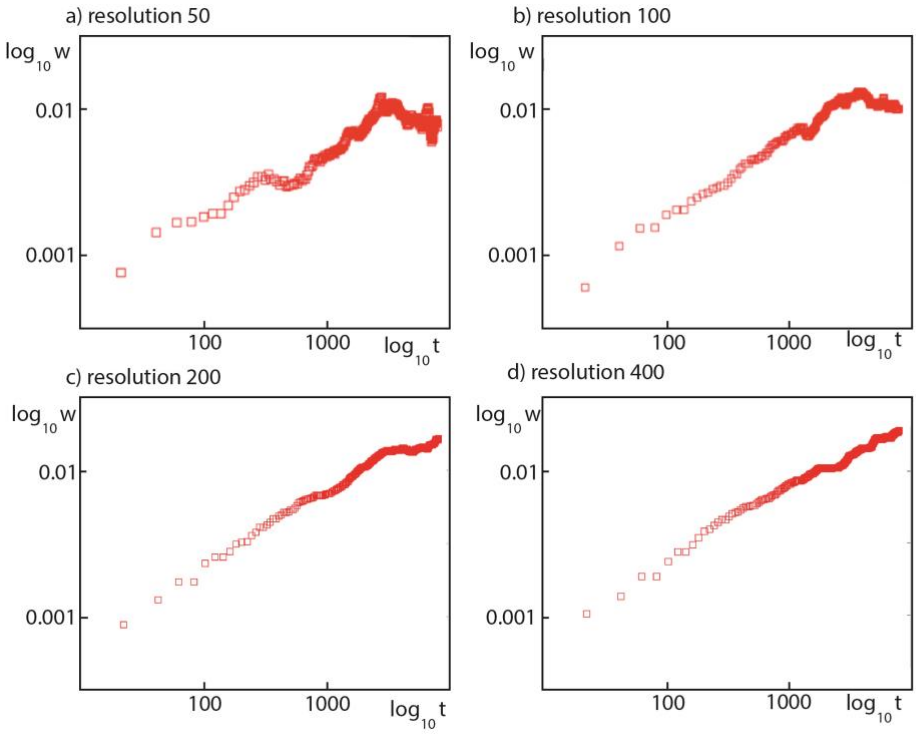

Fig. 4. Time series of simulated stylolites showing evolution of the average width of the interface through time in a log-log plot. a) early reached correlation length at resolution 50. b) correlation length is reached later at resolution 100. c) Correlation length at resolution 200 and d) Correlation length at resolution 400 barely reached. All figures are averages of 4 simulations

306 To attain a better picture we use equation 5 in Matlab to calculate the mean width of
307 modeled stylolites for different time steps (Fig. 4). This is done for resolutions 50,
308 100, 200 and 400 (particles in the x-direction) where for each plot in figure 4 the
309 results from four simulations are averaged. The initial development of the roughness
310 for all different resolutions is similar: the roughness grows as a function of time with
311 a given growth exponent. The simulations with resolution 50 start relatively early to
312 slow down in amplitude growth after about 30 time steps, then continue to grow and
313 become constant at around 300 time steps. Simulations with resolution 100 have a
314 more constant initial growth and become constant later than the ones with resolution
315 50 resulting in a larger final amplitude in roughness. The same pattern can be seen in
316 simulations with resolution 200 and 400, with an increase in resolution, the time when
317 the constant amplitude is reached is later and the final amplitude larger. In figure 5 all
318 simulations are included in one single graph illustrating that the growth exponent in
319 the initial regime is the same irrespective of resolution and that with an increase in
320 resolution the plateau in amplitude growth happens at a later time with a larger
321 amplitude. The inset in figure 5 shows a rescaled version of the larger figure where
322 the simulations with different resolutions plot on one single graph.

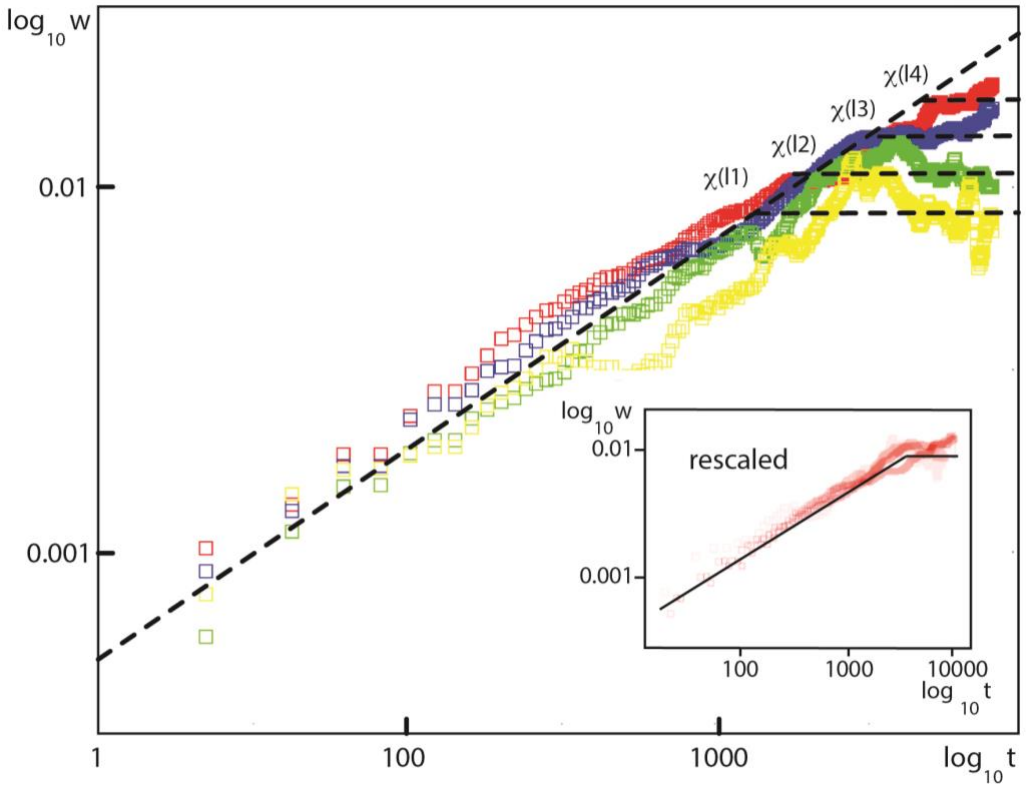

Fig. 5. Large plot showing all four modeled stylolite resolutions of Fig. 4 on top of each other illustrating the evolution of the average width of the interface through time in a log-log plot. The growth exponent β is the same for all resolutions but the correlation length as a function of the system size is reached later at larger system sizes. Inset shows a rescaled plot of the four curves where they collapse onto a single curve.

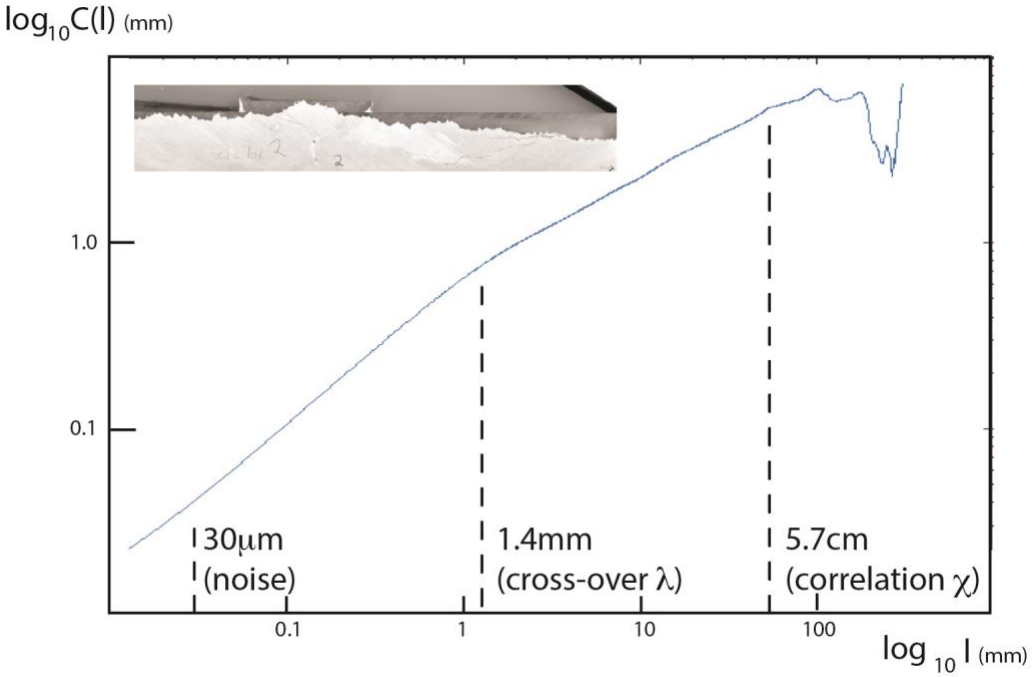

Fig. 6. Scaling of the natural stylolite of Fig. 1 using the correlation function. Plot shows the correlation C(l) (which is equivalent to the width of the stylolite interface) as a function of the correlation length l in log-log. The stylolite shows the two self-affine scaling regimes with a cross-over length λ of 1.4 mm and the correlation length χ at 5.7 cm when the amplitude becomes constant

3.2 Natural Stylolites

The natural stylolites can be used to show the scaling of the roughness for one single time step using the height-height correlation function (Fig. 6). One stylolite sample is shown as inset in figure 6 with a width of 30 cm scanned at a resolution of 10 μm per pixel. The correlation function shows two self-affine scaling regimes with an initial steep slope of about 1.0 until the cross-over λ is reached at about 1.4 mm followed by a second self-affine scaling regime with a lower slope of about 0.5. At 5.7 cm the slope changes again and becomes relatively flat until the correlation function reaches the system size. In order to be sure that this second cross-over is representing the correlation length χ as a function of time and thus compaction, we looked at the correlation functions for smaller parts of the same stylolite (Fig. 7). For widths of 30, 25 and 20 cm the position of the correlation length does not change. Between the system sizes 20, 15, 10 and 5 cm the correlation length progressively decreases.

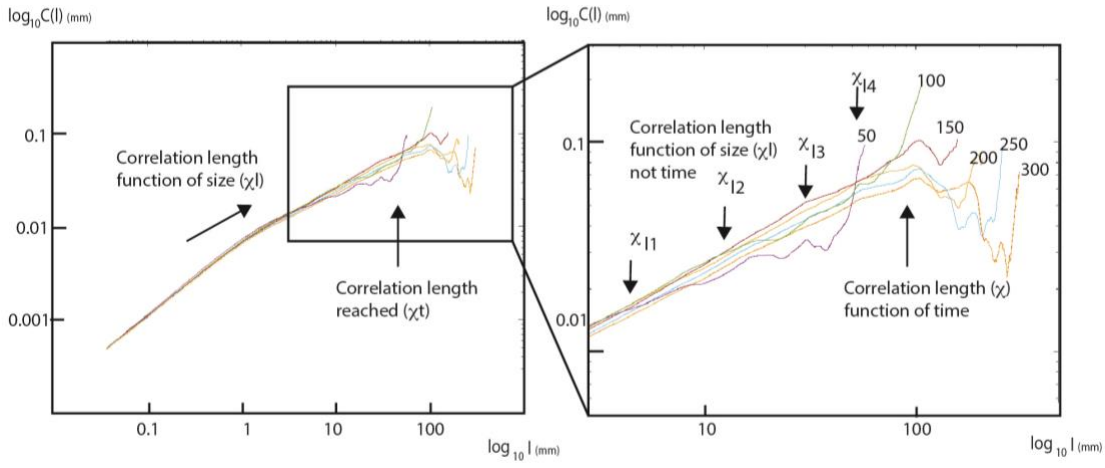

Fig. 7. Scaling of the natural stylolite of Figs. 1 and 6 using the correlation function for different lengths. Plot shows the correlation C(l) as a function of the correlation length l in log-log. a) shows the full plot and b) an inset of a). The correlation length stays constant for the three highest resolutions of 30, 25 and 20 cm showing that it is independent of the system size and thus a function of time. The three smaller resolutions show a decreasing correlation length at 15, 10 and 5 cm. Here the correlation length becomes a function of the system size

4. Discussion

4.1 scaling regimes in time and space

Figure 2 shows an overview of the scaling regimes that we expect to see in time and space. We will not be able to observe the time-series in natural stylolites because we typically see only one snapshot in time. Therefore we undertake the scaling analysis in time using numerical stylolites. Since the numerical stylolites are restricted in resolution in contrast to the natural ones we cannot see all three scaling regimes in time in one simulation. However, the numerical stylolites illustrate the transition between a self-affine time series with growth exponent β and the regime where the amplitude becomes constant. The growth exponent is about 0.5 meaning that the numerical stylolites are growing within the surface energy dominated regime. The length that separates the two regimes, the correlation length χ is evolving as a function of the system size in the numerical simulations as is illustrated in figures 2c and 5.

The natural stylolite (Fig. 6,7) offers the possibility to observe almost 5 orders of magnitude in scaling. The smallest system size is represented by the grain size at about 30 μm where the surface energy dominated regime starts with a self-affine roughness exponent α of about 1.0. This regime switches at the cross-over length λ of about 1.4 mm to a second self-affine roughness exponent of about 0.5 in the elastic energy dominated regime. At about 5.7 cm the correlation length χ is reached and the stylolite amplitude stops to increase. The correlation length should be a function of time and thus compaction at the stylolite. This is tested in figure 7 which illustrates that a variation of the system size from 30 to 25 and 20 cm does not change the position of the correlation length, hence it is independent on system size at that scale and is thus dependent on time. Below 20 cm the system size influences the position of

the correlation length, hence it is not dependent on time anymore but depends on the system size at that scale. This also means that samples of natural stylolites that have grown for the same amount of time (in terms of how much was dissolved at the stylolite) as our sample should be taken at sizes larger than 20 cm to observe a meaningful correlation length. Stylolites belong to a large class of systems that scale dynamically in space and time. The knowledge of the scaling behaviour of such systems offers a whole range of new applications in Earth Sciences and beyond to understand correlation in space and time as well as their use as stress inversion tools.

4.2 Compaction estimates

The natural stylolite example does allow to calculate the compaction on the stylolite using the correlation length (Laronne Ben-Itzhak et al., 2012). The compaction *A* on the stylolite can be calculated using the scaling function (eq. 3, Laronne Ben-Itzhak et al., 2012) as

$$A = a\left(\frac{\chi}{a}\right)^{z}, \qquad \text{eq. 9}$$

with *a* the grain size and *z* the dynamic exponent. However, the stylolite grows in two self-affine scaling regimes with different exponents, which is not taken care of in equation 9. We therefore propose to calculate the compaction for both regimes so that the overall compaction is the sum of the two regimes according to

$$A = a\left(\frac{\lambda}{a}\right)^{z_1} + \lambda\left(\frac{\chi}{\lambda}\right)^{z_2}, \qquad \text{eq. 10}$$

where the first part on the right hand side represents the surface energy dominated regime with the grain size *a* of 30 μm and the dynamic exponent z_1 of 2.0. This regime stops at the cross-over length λ. The second part of equation 7 on the right hand side represents the elastic energy dominated regime that starts at the cross-over length λ with the second dynamic exponent z_2 of 0.625 which stops at the cross-over

length χ. In summary, the calculation results in a compaction of 6.53 cm in the surface energy dominated regime, a compaction of 1.42 cm in the elastic energy dominated regime and an overall compaction of 7.95 cm. As was already discussed in Laronne Ben-Itzhak et al. (2012) this is only a rough estimate, however Koehn et al. (2016) found layer controlled stylolites that preserve the full dissolution in their teeth that where on that scale (4-6 cm).

4.3 Relative and absolute time scales and stress inversion

How does the correlation length relate to absolute time of the stylolite being active? Time with respect to the amount of dissolution determined through the scaling law and thus the correlation length is relative. In the models, the scaling law is dependent on the dissolution at the interface and thus related to a displacement rate of the boundary, which is rate controlling in the numerical model. In a stress controlled system, the slowest and thus rate controlling mechanism and its time scale will determine the absolute time, so either precipitation, transport or dissolution. One has to keep in mind, that the system may also switch from one to the other mechanism during stylolite growth. The scaling law is a function of the local dissolution at the interface and through that linked to absolute time. If this relation is linear, then the scaling law still works. If it is non-linear, for example the growth slows down with time, or the system switches between mechanisms with different time scales, then the scaling law is potentially skewed. The correlation length can be related to the amount of dissolution at the stylolite and through that it can be indirectly linked to absolute time. But in order to estimate this time we need to link the dissolution to the rate controlling mechanism. If this is known, there is a chance to estimate real time scales. Another possibility would be the existence of independent markers that can be dated, but this is probably rare in nature.

In terms of the stress inversion analysis on stylolites one has to note that the cross-over length-scale that is needed for the stress inversion is relatively stable. If the correlation length is below the cross-over length-scale, then stress inversion does not work (Fig. 2c l1 and l2 and Fig. 2d t1 and t2). However, with an increase in length and growth of the stylolite, the correlation length will evolve to be larger than the cross-over length-scale. From that point onwards the cross-over length-scale is stable and the stress inversion possible, unless the stress changes over time. The fact that the amplitude of the stylolite growth becomes stable in time and space does not effect the stress inversion, unless this is happening below the correlation length.

5. Conclusions

From our study the following conclusions can be reached:

a) Stylolites grow in three scaling regimes in space and time, two self-affine regimes with roughness exponents in space and growth exponents in time and a large scale regime where the roughness amplitude becomes constant.

b) Stylolites have three distinct length scales in space and time that separate the scaling regimes starting with the noise on the small scale, the cross-over length that is depending on stress and the correlation length that is depending on time in space series and on system size in time series.

c) Simulated stylolites show a Family-Vicsek scaling where the correlation length increases with system size.

d) The natural stylolites in this study show all three scaling regimes in the range of 10 μm to 30 cm with the grain size at 30μm, the cross-over length at 1.4 mm and the correlation length at 5.7 cm.

e) We propose a calculation of the compaction at the stylolite through time expanding the scaling law of Laronne Ben-Itzhak et al. (2012). Compaction is much larger (6.53 cm) in the surface energy dominated regime than in the elastic energy dominated regime (1.42 cm).

f) In order to find a meaningful correlation length in natural stylolites that is a function of time and thus compaction, in our example the sampling size has to be larger than 20 cm.

Systems that scale dynamically follow a Family-Vicsek scaling law where the correlation length increases with time. Determining this length thus gives an indication on the amount of time that the system was active. Exploring this length scale in other systems that potentially scale dynamically like fracture, fault and karst networks, hydrological system, ore deposits and geochemical networks and many others thus can offer new tools to understand their growth and connectivity. In addition, systems that include stress and surface energy may have an additional length scale similar to the cross-over in stylolites that can be explored for stress inversion analysis. We hope that the presented overview of dynamic scaling of stylolites promotes future of dynamic scaling of geological systems.

Acknowledgements

Comments by two anonymous reviewers and the guest editor Djordje Grujic are acknowledged, they improved an earlier version of the manuscript. We thank Tabea Platzer, Alexander Seute and Jacob Machleidt for very innovative method of preparing the samples. This research was funded within the scope of the project “Integrated geophysical-structural-kinematic analysis of the fault patterns in Northern Bavaria” by the Bayerisches Landesamt für Umwelt (LfU) and by the Bavarian Ministry of Science and Art (StMWK) funded project "langfristig" of the Geothermal Alliance Bavaria (GAB) which is gratefully acknowledged, as well as the “Dr. Hertha and Helmut Schmauser-Stiftung” of FAU University. This work was partly supported by the Research Council of Norway through its Centers of Excellence funding scheme, project number 262644.

References

Allen, D. N. de G., 1954, Relaxation Methods: New York, McGraw Hill, 257 p.

Barabasi, A.L., Stanley, H.E., 1995. Fractal Concepts in Surface Growth. Cambridge University Press.

Beaudoin, N., Koehn, D., Lacombe, O., Lecouty, A., Billi, A., Aharonov, E. & Parlangeau, C. 2016. Fingerprinting stress: Stylolite and calcite twinning paleopiezometry revealing the complexity of progressive stress patterns during folding-The case of the Monte Nero anticline in the Apennines, Italy. Tectonics 35, 1687–1712.

Beaudoin, N. and Lacombe, Ol, 2018. Recent and future trends in paleopiezometry in the diagenetic domain: Insights into the tectonic paleostress and burial depth history of fold-and-thrust belts and sedimentary basins. Journal of Structural Geology, 114, 357-365.

Beaudoin, N., Gasparrini, M., David, M.-E., Lacombe, O., Koehn, D., 2019. Bedding-parallel stylolites as a tool to unravel maximum burial depth in sedimentary basins: Application to Middle Jurassic carbonate reservoirs in the Paris basin, France. GSA Bull. 131, 1239–1254.

Beaudoin, N., Labeur, A., Lacombe, O., Koehn, D., Billi, A., Hoareau, G., Boyce, A., John, C.M., Marchegiano, M., Roberts, N.M., Millar, I.L., Claverle, F., Pecheyran, C., Callot, J-P, 2020a. Regional-scale paleofluid system across the Tuscan Nappe–Umbria–Marche Apennine Ridge (northern Apennines) as revealed by mesostructural and isotopic analyses of stylolite–vein networks**.** Solid Earth, 11, 1617-1641.

Beaudoin, N., Lacombe, O., David, M-E, Koehn, D., 2020b. Does stress transmission in forelands depend on structural style? Distinctive stress magnitudes during Sevier thin-skinned and Laramide thick-skinned layer-parallel shortening in the Bighorn

512 Basin (USA) revealed by stylolite and calcite twinning paleopiezometry. Terra
513 Nova, 32, 3, 225-233.
514 Beaudoin, N., Lacombe, O., Koehn, D., David, M.-E., Farrell, N., and Healy, D.
515 2020c. Vertical Stress History and Paleoburial in Foreland Basins Unravelled by
516 Stylolite Roughness Paleopiezometry: Insights from Bedding-Parallel Stylolites in
517 the Bighorn Basin, Wyoming, USA. *J. Struct. Geology.*136, 104061.
518 doi:10.1016/j.jsg.2020.104061
519 Bertotti, G., de Graaf, S., Bisdom, K., Oskam, B., Vonhof, H.B., Bezerra, F.H.,
520 Reijmer, J.J., and Cazarin, C.L., 2017. Fracturing and fluid-flow during post-rift
521 subsidence in carbonates of the Jandaíra Formation, Potiguar Basin, NE Brazil:
522 Basin Research, v. 29, p. 836-853.
523 Bons, P.D., Koehn, D., Jessell, M.W., 2008. Microdynamics Simulation. Springer
524 Lecture Series in Earth Sciences, pp. 406.
525 Ebner, M., Koehn, D., Toussaint, R., Renard, F., Schmittbuhl, J. 2009a. Stress
526 sensitivity of stylolite morphology. Earth and Planetary Science Letters 277(3-4),
527 394-398.
528 Ebner, M., Koehn, D., Toussaint, R., Renard, F. 2009b. The influence of rock
529 heterogeneity on the scaling properties of simulated and natural stylolites. Journal
530 of Structural Geology 31(1), 72-82.
531 Ebner, M., Toussaint, R., Schmittbuhl, J., Koehn, D., Bons, P. 2010a. Anisotropic
532 scaling of tectonic stylolites: A fossilized signature of the stress field? Journal of
533 Geophysical Research: Solid Earth115 (6), B06403.
534 Ebner, M., Piazolo, S., Renard, F., Koehn, D. 2010b. Stylolite interfaces and
535 surrounding matrix material: Nature and role of heterogeneities in roughness and
536 microstructural development. Journal of Structural Geology 32(8), 1070-1084.

Family, F., & Vicsek, T., 1985. Scaling of the active zone in the Eden process on percolation networks and the ballistic deposition model. Journal of Physics A: Mathematical and General, 18(2), L75.

Heap, M., Reuschlé, T., Baud, P., Renard, F., Iezzi, G., 2018. The permeability of stylolite-bearing limestone. J. Struct. Geol. 116, 81–93.

Kley, J. & Voigt, T. 2008. Late Cretaceous intraplate thrusting in central Europe: Effect of Africa-Iberia-Europe convergence, not Alpine collision. Geology 36, 839-842.

Koehn, D., Renard, F., Toussaint, R., Passchier, C.W. 2007. Growth of stylolite teeth patterns depending on normal stress and finite compaction. Earth and Planetary Science Letters 257 (3-4), 582-595

Koehn, D., Ebner, M., Renard, F., Toussaint, R., Passchier, C.W. 2012. Modelling of stylolite geometries and stress scaling. Earth and Planetary Science Letters 341, 104-113.

Koehn, D., Rood, M.P., Beaudoin, N., Chung, P., Bons, P.D., Gomez-Rivas, E., 2016. A new stylolite classification scheme to estimate compaction and local permeability variations. Sediment. Geol. 346, 60–71.

Labeur, A., Beaudoin, N.E., Lacombe, O., Emmanuel, L., Petracchini, L., Daëron, M., Klimowicz, S. and Callot, J.-P., 2021. Burial-deformation history of folded rocks unraveled by fracture analysis, stylolite paleopiezometry and vein cement geochemistry: A case ctudy in the Cingoli Anticline (Umbria-Marche, Northern Apennines)n, Geosciences, 11, 135.

Laronne Ben-Itzhak, L., Aharonov, E., Toussaint, R., Sagy, A., 2012. Upper bound on stylolite roughness as indicator for amount of dissolution. Earth Planet. Sci. Lett. 337–338, 186–196.

562 Martín-Martín, J.D., Gomez-Rivas, E., Gómez-Gras, D., Travé, A., Ameneiro, R.,
563 Koehn, D., Bons, P.D., 2018. Activation of stylolites as conduits for overpressured
564 fluid flow in dolomitized platform carbonates. In: Ashton, M., Dee, S.J.,
565 Wennberg, O.P., Eds.: Subseismic-scale reservoir deformation: introduction. Geol.
566 Soc. London, Spec. Publ. 459, pp. 157–176.
567 Morad, D., Nader, F.H., Morad, S., Al Darmaki, F., Hellevang, H., 2018. Impact of
568 Stylolitization On Fluid Flow and Diagenesis in Foreland Basins: Evidence from
569 an Upper Jurassic Carbonate Gas Reservoir, Abu Dhabi, United Arab Emirates. J.
570 Sediment. Res. 88(12), 1345-1361.
571 Park, W. C., Schot, E. H. 1968. Stylolites; their nature and origin. Journal of
572 Sedimentary Research, 38(1), 175-191.
573 Piazolo, S., Bons P.D., Griera, A., Llorens, M-G., Gomez-Rivas, E., Koehn, D.,
574 Wheeler, J., Gardner, R., Godinho J.R.A., Evans, L., Lebensohn, R.A., Jessell,
575 M.W., 2019. A review of numerical odelling of the dynamics of microstructural
576 development in rocks and ice: Past, present and future. Journal of Structural
577 Geology 125, 111-123.
578 Renard, F., Schmittbuhl, J., Gratier, J.-P., Meakin, P., and Merino, E. 2004. Three-
579 dimensional roughness of stylolites in limestones. Journal of Geophysical
580 Research-Solid Earth 109, doi:10.1029/2003JB002555
581 Rispoli, R., 1981. Stress-fields about strike-slip faults inferred from stylolites and
582 tension gashes. Tectonophysics 75, 29–36.
583 Rolland, A., Toussaint, R., Baud, P., Schmittbuhl, J., Conil, N., Koehn, D., Renard,
584 F., Gratier, J. P. 2012. Modeling the growth of stylolites in sedimentary rocks.
585 Journal of Geophysical Research-Solid Earth 117(6), B06403.

586 Rolland, A., Toussaint, R., Baud, P., Conil, N., Landrein, P., 2014 Morphological
587 analysis of stylolites for paleostress estimation in limestones, International Journal
588 of Rock Mechanics and Mining Sciences 67, 212-225.
589 Schmittbuhl, J., Renard, F., Gratier, J.P., Toussaint, R., 2004 Roughness of stylolites:
590 Implications of 3D high resolution topography measurements. Physical Review
591 Letters 93 (23), 238501, doi:10.1103/PhysRevLett.93.238501
592 Stockdale, P. B. 1922. Stylolites: their nature and origin. Indiana University Studies 9,
593 1-97.
594 Toussaint, R., Aharonov, E., Koehn, D., Gratier, J.P., Ebner, M., Baud, P., Rolland,
595 A., Renard, F., 2018. Stylolites: A review. J. Struct. Geol. 114, 163-195.
596

597 **Figure captions**

598 Figure 1 a) Geological overview map of the sampling area with the Kulmbach reverse
599 fault that displaces Triassic against Jurassic units. b) Sampling of tectonic stylolites in
600 a Jurassic (Malm) limestone quarry in the Franconian Alb next to the Kulmbach fault
601 near Kirchleus (50º10'49"N, 11º22'11"E) in SE Germany. c) 30 cm long slab that
602 was used for the analysis. The sample is first prepared with epoxy and then cut to
603 preserve the teeth. d) close up view of the stylolite surface under a digital microscope.
604 Figure 2 Stylolite scaling in self-affine time and space series. a) time-series with three
605 scaling regimes, two self-affine regimes with growth exponents β and a third regime
606 where the stylolite width becomes constant. b) space-series with the same three
607 scaling regimes where the two self-affine regimes are now characterized by the
608 roughness exponent α. c) evolution of the correlation length χ as a function of system
609 size l in the time-series. d) evolution of the correlation length χ as a function of time t
610 in the space-series. Compilation of data and graphs from Barabasi and Stanley (1995),

611 Koehn et al. (2007), Ebner et al. (2010b), Laronne Ben-Itzhak et al., (2012) and
612 Toussaint et al. (2018).
613 Figure 3 Simulated stylolite with a resolution of 100 particles in x. The box is
614 compacted vertically with a displacement controlled boundary. Particles can dissolve
615 at an initially flat interface in the middle of the box as a function of local changes in
616 elastic and surface energy as well as normal stress. Roughening develops during
617 dissolution of particles as a function of a variation in dissolution constants. a) 100, b)
618 1000, c) 2000, d) 3000, e) 4000 and f) 5000 compaction steps. The large box shows
619 the roughness evolution within the box as a function of time/compaction steps (t1-t6).
620 The correlation length is reached at e) when the amplitude growth stops. In f) two
621 boxes at length scale l1 and l2 are shown with the smaller box showing an earlier
622 reached correlation length and thus a smaller amplitude within the box.
623 Figure 4 Time series of simulated stylolites showing evolution of the average width of
624 the interface through time in a log-log plot. a) early reached correlation length at
625 resolution 50. b) correlation length is reached later at resolution 100. c) Correlation
626 length at resolution 200 and d) Correlation length at resolution 400 barely reached.
627 All figures are averages of 4 simulations.
628 Figure 5 Large plot showing all four modeled stylolite resolutions of figure 4 on top
629 of each other illustrating the evolution of the average width of the interface through
630 time in a log-log plot. The growth exponent β is the same for all resolutions but the
631 correlation length as a function of the system size is reached later at larger system
632 sizes. Inset shows a rescaled plot of the four curves where they collapse onto a single
633 curve.
634 Figure 6 Scaling of the natural stylolite of figure 1 using the correlation function. Plot
635 shows the correlation *C(l)* (which is equivalent to the width of the stylolite interface)

as a function of the correlation length *l* in log-log. The stylolite shows the two self-affine scaling regimes with a cross-over length λ of 1.4mm and the correlation length χ at 5.7 cm when the amplitude becomes constant.

Figure 7 Scaling of the natural stylolite of figures 1 and 6 using the correlation function for different lengths. Plot shows the correlation *C(l)* as a function of the correlation length *l* in log-log. a) shows the full plot and b) an inset of a). The correlation length stays constant for the three highest resolutions of 30, 25 and 20cm showing that it is independent of the system size and thus a function of time. The three smaller resolutions show a decreasing correlation length at 15, 10 and 5cm. Here the correlation length becomes a function of the system size.